Robles Muñoz, G., Shafiq, M., & Martínez Tarifa, J. M. (2019). Multiple Partial Discharge Source Localization in Power Cables through Power Spectral Separation and Time-Domain Reflectometry. IEEE Transactions on Instrumentation and Measurement, 68(12).

DOI: 10.1109/TIM.2019.2896553

Multiple partial discharge source localization in power cables through power spectral separation and time-domain reflectometry

Guillermo Robles, *Senior Member, IEEE,* Muhammad Shafiq, *Member, IEEE,* and Juan Manuel Martínez-Tarifa, *Senior Member, IEEE,*

***Abstract*—Insulated power cables are becoming increasingly popular in today's developing distribution and transport networks. However, due to ageing, deterioration and various operational and environmental stresses, insulation defects may appear so the cable needs to be monitored timely to avoid unexpected failures. Most of these defects are responsible for partial discharge (PD) activity. The localization of the sources of these discharges is a highly decisive facet in the condition-based monitoring of power cables. The techniques for the localization of single PD defects in insulated power cables are well presented in the current bibliography. However, when several simultaneous PD sources are active, the localization of the sources becomes quite complex. This paper develops an efficient technique for the separation and localization of multiple PD sources in a medium voltage (MV) cable. The experimental results are obtained with single-end based measurements using a high frequency current transformer (HFCT) in a laboratory environment. The data processing based on the spectral characteristics of the signals is carried out by using the power ratios (PR) technique in order to determine the presence of different types of PD. Once the signals are separated, the PD sources can be localized with an individualized analysis of each source through time domain reflectometry (TDR). The proposed methodology can be very valuable to improve the location diagnostic capability of the condition-based monitoring solutions especially for underground cables.**

***Index Terms*—Condition monitoring, time domain reflectometry, signal characterization, partial discharges, particle swarm optimization, signal propagation, power cables, spectral power ratios.**

I. Introduction

THE growing use of underground cables in medium voltage networks is not only improving the reliability of the power grid but it is also being demanded due to esthetic, environmental and operational constraints. It is especially important to bear in mind that new high-voltage direct current (HVDC) line projects are continuously being developed to increase the power delivery capability of electrical systems, as it is the case, for example, for new offshore wind energy generation facilities, or increased interconnections between European countries [1], [2]. This expansion in the use of underground and submerged cables is also raising the challenges of their maintenance that need more sophisticated and accurate solutions [3].

Polyethylene-based materials, typically used as insulation for these type of assets, are quite sensitive to degradation. Therefore, the maintenance of insulated power cables is a key point for utilities to ensure the quality and continuity of the power delivery so they are manufactured with high-quality standards where tests guarantee their flawless performance [4], [5]. In general, the insulation of high-voltage equipment is subjected to several stresses that can degrade its performance and, in the case of power cables, their transmission capability. In addition to the high electrical fields applied to their insulation systems, thermal, mechanical and environmental stresses contribute significantly to their accelerated ageing [6]. Many of these degrading agents lead to the appearance of partial discharges (PD), defined as small energy ionization processes occurring in sites where the applied electric field is highly inhomogeneous [7]. In the particular case of insulated power cables, these discharges can be found in joints between sections of cable or between cable and electrical machines, and in the main body of the cable due to mechanical stresses during its layout or works done during its lifetime [8]. These events degrade the insulation system further, so its detection is mandatory for the diagnosis of causes and consequences of the insulation degradation [9], [10]. In fact, the operation of the cable in real conditions and its installation (mechanical deformation is possible, joints can be defective...) can cause cracks or voids where PD will eventually arise [11], [12] which would cause a total breakdown in short operation times. As these cables are usually buried or submerged for long distances, efficient diagnostic techniques are paramount to improve the performance of the repairing activities by focusing the maintenance on a limited area [13].

Conventionally, PD diagnostics consist on the detection and identification of the pulses, the localization of their sources and the quantification of the degree of damage [14]–[16]. The digital advancements in this area has brought the identification and classification tasks, that were being done on the back end before, to the front end of the diagnostic framework. This paper is focused on the detection, identification of the number of sources of partial discharges, and localization tasks. An ample amount of research has been going on the

G. Robles and J.M. Martínez-Tarifa are with the Department of Electrical Engineering, Universidad Carlos III de Madrid, Leganés, 28911 Spain e-mail: (see http://electrica.uc3m.es/grobles).

Muhammad Shafiq is with the Department of Electrical Engineering, University of Vaasa, Finland.

investigation of the multiple PD faults initiated by different types of PD sources in machines and power cables [17], [18]. The developed techniques are used to detect and identify the presence of the multiple PD sources such as corona, discharges in oil, surface discharges, or internal discharges using phase-resolved PD (PRPD) patterns when possible. These patterns require a synchronization signal from the power grid (50 or 60 Hz) that is not always available and, in the particular case of HVDC lines, this analysis could not be done.

The localization of single defects along a cable has traditionally been done using the observations of the time of arrival (ToA) of the original PD pulse and its subsequent reflections to the sensors, the wave propagation speed and the total length of the cables [19], [20]. This time domain reflectometry (TDR) technique is usually implemented using one-end measurements (single sensor) or two-ends measurements (two sensors) [21], [22]. A combined use of TDR and frequency domain reflectometry (FDR) has also been proposed to improve the localization capabilities of the TDR [23]. Since the reference signals are damped and dispersed along the cable, they carry the localization information in both the time and frequency domains. Therefore, in this method, a chirp signal with a central frequency and bandwidth designed according to the characteristics of the cable is injected in one end substituting the pulsed signal of TDR. The distance to the fault can be calculated through the Euclidean distance between the transformation of the reference signal and the reflected signals in the time-frequency domain. In all the aforementioned works the sensors are always inductive sensors in the high-frequency (HF) range from 3 MHz to 30 MHz. There has also been an attempt to use an array of distributed ultra high frequency (UHF) sensors along the cable [24] but this would be only applicable to short lengths since the cables are shielded and the antennas would only detect the emission of the fault travelling through the air. Other methods based on interferometric fiber optic sensors to localize the acoustic emission of the PD have also been proposed for long length cables [25].

However, when two or more PD sources are active simultaneously on a cable section, the sensor/s at the end/s of the cable capture the original PD signals indiscriminately together with the reflected pulses propagating along the line which makes the implementation of the location techniques a very complex task. These measured signals should be separated from one another in order recognize the presence of more than one PD source and then apply the localization algorithm to each source. In [24] the separation of different types of sources is previously done plotting the PRPD pattern and classifying the signals in a time-frequency map. However, the authors claim that, due to the mismatch between the impedance of the cable and the terminating impedance causing reflections and attenuation, the time domain reflectometry cannot be effectively used in cables with two sources.

This paper proposes an effective approach to the separation and localization of two or more simultaneous PD sources in power cables with single-end measurements using a high frequency current transformer (HFCT). The proposal is based on the well known fact ([15], [24], [26]) that any pulse inherits a fingerprint associated to the site in which the partial discharge occurs and the characteristics of the transmission line from that site to the sensor. Therefore, a spectral characterization of the PD pulses needs to be done through the spectral power ratios (PR) technique to determine the number of sources [26], [27]. Thus, a previous separation of the detected PD events will be made with these PR data, which will be used to focus on each type of defect. The experimental measurements in the paper show three simultaneous sources that should be separated. One of the classes is related with the electrical noise, while the other two are PD sources whose reflections will used for their localization. Finally, once each PD source is isolated, the localization can be made just analyzing the ToA data set for each source and applying time domain reflectometry. Precisely, here lies the novelties of this paper when compared to our past works: first, the signals analyzed are no longer individual pulses but the original pulse propagated through a cable and the subsequent reflections at both ends. Therefore, it is necessary to test if the transformation of the signals to the frequency domain is still sufficient to separate them. Second, since all pulses are propagated along the same cable, the contribution of the characteristics of the transmission line to their wave shape in terms of attenuation, dispersion and frequency content is very similar for all of them. Therefore, it is not immediate to assume that it is possible to separate events attending exclusively to the spectral characteristics of the propagated signals. And, finally, the method is tested in a different asset with the aim of studying the propagation of signals and localization of the source of partial discharges instead of characterizing them in phase-resolved PD patterns.

II. Pulse source separation through spectral power ratios

Since partial discharges are sudden changes of charge inside voids in the dielectric, the effect is a current pulse that travels through the conductor and the insulation to ground. The energy is emitted in the electromagnetic spectrum from the high frequency band (HF) to the ultra high frequency band (UHF) so it can be detected with broadband instrumentation such as high-frequency current transformers (HFCT) and antennas, respectively. In general, the time domain characteristics of the original PD, namely, rise and fall times and amplitude of the pulse, depend on the type of defect and the charge involved in the avalanche. Then, the pulse propagates along the cable and it is modified by the characteristics of the lossy transmission line until it reaches a sensor. The consequence is that the transmission line has great influence on the spectrum of the PD adding its new frequency components. Nevertheless, even with the influence of the transmission line, different types of pulses can be identified using their spectral components and, then, studied individually to find their origin. Moreover, the characteristics of noise show also a different fingerprint that can be used to separate it from the events of interest.

In order to make a systematic separation, the authors proposed the spectral power ratios (PR) in several previous works [26], [27]. This technique calculates the spectral power of the detected signals in two frequency bands, one at lower frequencies $[f_{1L}, f_{2L}]$ and the other one at higher ones $[f_{1H}, f_{2H}]$.

In order to make these variables independent from the signal power or amplitude, these spectral powers are divided into the overall spectral power of the signal through the complete studied bandwidth, $[0, f_T]$. Thus, the resulting spectral Power Ratios (PR) for low and high frequencies (PRL and PRH respectively) are calculated using the following Equations (1) and (2):

$$PRL = \frac{\sum_{f=f_{1L}}^{f_{2L}} |G(f)|^2}{\sum_{f=0}^{f_T} |G(f)|^2} \quad (1)$$

$$PRH = \frac{\sum_{f=f_{1H}}^{f_{2H}} |G(f)|^2}{\sum_{f=0}^{f_T} |G(f)|^2} \quad (2)$$

where $G(f)$ is the Fourier transform of the signal to characterize $g(t)$ and f_T is the highest frequency of interest of $g(t)$. The frequencies f_{1L}, f_{2L}, f_{1H}, f_{2H}, and f_T can be configurable by an analyst according to the characteristics of $G(f)$, complying with the conditions $0 \leq f_{1L} \leq f_{2L}$, $f_{1H} < f_{2H} \leq f_T$, and $f_{1L} < f_{2H}$. These two parameters are used to characterize each signal detected by the instrumentation system. This is done by means of a 2-dimensional representation of both parameters, which is known as the PR map. The main idea of the technique is to represent each detected signal in the PR map. Signals with similar shape in their spectra, will be represented in a specific region of the PR map forming a cluster, whereas signals with different spectra, will form a different cluster. All previous works have shown that this technique is successful in high-voltage applications for the separation of different physical phenomena or similar phenomena which take place at different distances from the sensors [26], [27]. Since the selection of the proper frequency intervals for the calculation of PRL and PRH can be complex in certain circumstances or the optimum separation between the phenomena cannot be achieved with the simple visual inspection of the spectra, the authors proposed the use of an unsupervised system which increased the distance between clusters by means of particle swarm optimization (PSO), [28].

III. Maximizing the Distance Between Clusters with Particle Swarm Optimization

The selection of a pair of appropriate intervals of frequency $[f_{1L}, f_{2L}]$ and $[f_{1H}, f_{2H}]$ will make that those signals corresponding to the same event would form a packed cluster when represented in a two dimensions scatter plot PRL versus PRH. Other events with different spectral characteristics would have differences in these parameters, so the clusters would be plotted in another region of the map. There would be as many clusters as types of signals. Therefore, the aim of the optimization algorithm would be to have a certain pair of frequency intervals to represent similar events in a map in the form of a packed group that is clearly separated from other groups maximizing the distance between their centroids. Currently, the clusters are selected using the k-means algorithm but other more sophisticated techniques can be applied in which the initial number of types of signals is not known. The distance between the centroids of clusters i and j and the scatter of the data within each cluster are calculated with the Mahalanobis distance m_{ij}, then, the objective function M would maximize the minimum distance between the centroids [28]:

$$M = \max \min_{i \neq j}^{k} m_{ij} \quad (3)$$

Particle swarm optimization (PSO) has been chosen as the technique to obtain M through the exploration of sets of frequency intervals.

PSO is a metaheuristic algorithm with hive intelligence based on the behaviour of a flock of birds or a school of fish pursuing a prey. The algorithm is initialized deploying a defined set of N particles in the solutions space and calculating their positions in every iteration towards an optimum. The dimension of this space depends on the characteristics of the problem. In our case, there are four parameters, $[f_{1L}, f_{2L}]$ and $[f_{1H}, f_{2H}]$, that set the conditions for the optimization function, M. Therefore, every particle would have a position in the four-dimensions solution space and will be directed to a final position that will determine the best set of frequency intervals to separate the clusters in the PR map.

In every iteration l, the movement of every particle is computed based on the distance of that particle to its personal best solution for M, $\mathbf{P_{n,b}}$, and the distance to the overall best solution for M, $\mathbf{P_b}$. These distances are multiplied by two coefficients, c_1 and c_2 to weigh the effect in the optimization function of the individual or social influence, respectively. Thus, the position $\mathbf{P_n}$ and the speed of movement of particle n, $\mathbf{v_n}$, are evaluated with the following standard PSO algorithm:

$$\begin{aligned} \mathbf{v_n}(l+1) &= \mathbf{v_n}(l) + c_1 \mathbf{U_1}(0,1) \otimes [\mathbf{P_{n,b}}(l) - \mathbf{P_n}(l)] \\ &+ c_2 \mathbf{U_2}(0,1) \otimes [\mathbf{P_b}(l) - \mathbf{P_n}(l)], \\ \mathbf{P_n}(l+1) &= \mathbf{P_n}(l) + \mathbf{v_n}(l+1), \end{aligned} \quad (4)$$

where $\mathbf{U_1}(0,1), \mathbf{U_2}(0,1) \in [0,1]^4$ are four-dimensional random vectors, with each component independently obtained from a uniform distribution between 0 and 1. Both vectors, together with the coefficients c_1 and c_2, randomize the movement of the particles towards their own best and the swarm's best, respectively.

Once the movement of all N particles has been calculated, the parameters PRH and PRL are evaluated for all the acquired signals using the N sets of four frequencies that conform the intervals, see the flowchart in Figure 1. The points in the PR map are grouped in clusters with the k-means algorithm and the distances between centroids are then computed. The personal best and overall best of Equations (4) are updated with the results of these distances and the process is repeated until an optimum is reached or a maximum number of iterations is reached. The outcome of the algorithm after a certain number of iterations is a set of frequencies that maximizes the distance between clusters.

IV. Experimental Setup

In this work, all measurements were conducted in a 20 kV shielded MV cable with a low density high molecular weight polyethylene (LDHMW PE) insulation. The length of the cable

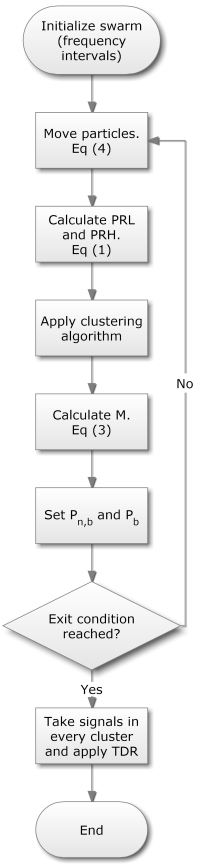

Fig. 1: Flowchart of the process followed to maximize the distance between clusters with PSO and PR maps.

is 150 m, the conductor section is AWG 18 or $1\ \mathrm{mm}^2$ and the external jacket has a diameter of 7.7 mm.

The cable under test was new and it was the first time that it had been brought to operation, therefore the ends (end A and end B) of the cable were peeled off showing the shielding and the inner conductor. The end B was immersed in a vessel with transformer oil to avoid to have unnecessary partial discharges. The inner conductor at end A was connected to a high-voltage source with enough power to feed the capacitive current of the cable and the shielding was grounded. At this end, a high-frequency current transformer with a bandwidth up to 80 MHz and a sensitivity of 5 V/A was clamped to the ground connection and its output was connected to a high-speed digital storage oscilloscope (DSO) with a bandwidth of 2.5 GHz and a maximum sampling frequency of 10 GSps per channel. In addition, a 1 nF coupling capacitor was connected to the measuring branch as suggested by the standard IEC 60885-3 [4]. This setup is commonly used to detect PD in electrical insulation, which can always be modeled as an equivalent capacitance. Thus, the coupling capacitor and the insulation become a low-impedance mesh for the high-frequency impulses created by the discharges [7]. The high voltage source has the possibility to vary the input supply to adjust the voltage at a desired level. Since these cables are built to avoid PD within their main body, [4], partial discharges would only happen at end A, would travel forward towards

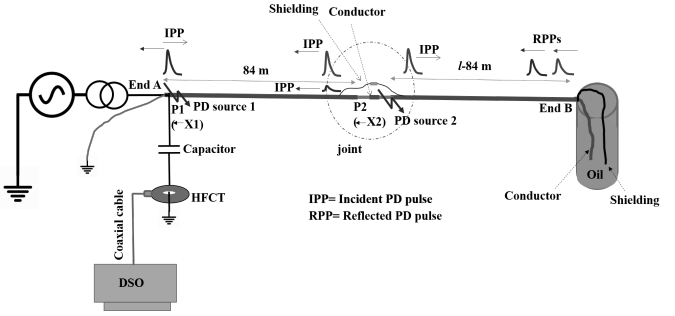

Fig. 2: Layout of the experimental setup for the localization of two fault sources in the cable. The PD source 1 was at end A and the PD source 2 at a distance $x = 84$ m from end A.

end B and would be reflected backwards to end A until the pulse is completely damped. This setup was used to compare the speed of propagation in the cable obtained experimentally with its theoretical value.

Then, the cable was split into two sections, see Figure 2, and connected again at point P2 joining the inner conductors and connecting the shielding with crocodile clips. This creates an intentional defect in the electrical insulation between conductor and shielding. The result is a point in the middle length of the cable where partial discharges can occur when the voltage is high enough. Section 1 goes from end A to point P2 and section 2 from point P2 to end B. Finally, since end A in section 1 was peeled, it is expected to have two different sources of partial discharges. The overall setup would be the former cable 150 m long with a defect at 84 m from the high-voltage connection and an open-end at the end of section 2. This open-end represents an infinite impedance that will reflect any pulses generated along the cable.

Notice that PD are fast current transients happening between the capacitive coupling between the internal conductor and the shielding connected to ground. When the cable is split, the shielding is interrupted and the inner conductor is exposed so there appears a direct capacitive coupling between the metallic ground plane of the laboratory and the inner conductor. If the cable is laid close to the ground plane, this capacitive coupling becomes very effective and the current pulse would follow two paths: along the long path of the cable towards both ends finally reaching the HFCT as expected and through the ground plane towards the HFCT following a very short distance of about 2 meters. This means that the signals acquired by the HFCT would be both the pulse of interest that travels along the cable and the direct pulse through ground altering the results. Therefore, the cable was carefully laid separating from ground the sections with the inner conductor exposed eliminating the direct transmission of the PD pulse.

V. Implementation of the Proposed Technique on Measured PD Signals

A. Characterization of the cable

A precise information of the wave propagation speed plays a key role to improve the accuracy of the location of PD defects along the cable. The propagation speed of electromagnetic

signals in vacuum is $c = 3\times10^8$ m/s. However, while traveling along the cables, the medium between the conductor and the shielding is a dielectric material that reduces the wave propagation speed so it has to be determined with Equation (5) where ϵ_r is the relative permittivity of the dielectric.

$$v = \frac{c}{\sqrt{\epsilon_r}} \tag{5}$$

Equation (6) determines the capacitance per unit length of a long cylindric capacitor with internal diameter d_1, external diameter d_2 and dielectric with permittivity $\epsilon = \epsilon_0\epsilon_r$.

$$C_l = \frac{2\pi\epsilon}{\log(d_2/d_1)} \tag{6}$$

According to the data sheet of the cable the capacitance per unit length is $C_l = 121$ pF/m, and the dimensions are $d_1 = 1.24$ mm, $d_2 = 6.9$ mm, yielding a relative permittivity of the dielectric $\epsilon_r = 3.73$. Therefore, the speed of propagation in the cable is $v = 1.55 \times 10^8$ m/s.

The capacitance of the cable was measured with a capacitance and dissipation factor ($\tan\delta$) measuring system based on an AC bridge to obtain a total value of $C = 17.8$ nF, therefore, $C_{lm} = 118.7$ pF/m since the length of the cable is $l = 150$ m. The difference between the experimental capacitance per unit length C_{lm} and the one given by the manufacturer C_l is less than 2 % so we can assume that the speed of propagation has been correctly calculated.

Nevertheless, a direct experimental measurement of the speed was also conducted in the whole cable, before creating the defect, calculating the time difference between the incident and the reflected pulse of a partial discharge and applying time domain reflectometry (TDR). During the characterization, the voltage was raised until partial discharges appeared in end A and it was observed that the PD activity was guaranteed above 3 kV which was set as the PD inception voltage (PDIV). The sampling frequency of the oscilloscope, f_s was set to 1 GS/s (the sampling time, $T_s = 1$ nanosecond) and the time window to 5 µs yielding 5000 samples per signal. This time window was set to a value that allowed to register the first arriving signal and the reflections which were spaced every 1.905 microseconds which is compatible with PD generated at end A. This value is an averaged quantity obtained with the cursors in the oscilloscope from 8 different signals. Considering the length of the cable $l = 150$ m, it was possible to determine the speed of propagation to be $v_m = 1.575 \times 10^8$ m/s or 52.5% of c. Considering that the reflections were separated close to 2 microseconds, the time window in the oscilloscope was set to 5 microseconds so we could see the first arriving signal and two reflections. The third reflection was too attenuated to be of interest.

This result is very close to the speed given by Equations (5) and (6), the difference is only 1.6 %, so it will considered as the speed of propagation henceforth. These experiments also determined that there is a source of partial discharges at end A.

B. Separation of the signals in the case of multiple sources

Once the cable has been characterized the next step is to obtain partial discharges from the two sources in the cut cable of Figure 2. The trigger was set to very low voltage levels to acquire all type of signals, even noise. Then, the voltage was raised above the PDIV of the defect at end A up to 4.2 kV and 500 signals were acquired. Then, all pulses whose maxima were above a threshold were not considered so we could be sure that no pulses were clipped during the acquisition which would add distortion to the analysis in frequency. This threshold was set to 30 mV so the signals analyzed with the algorithms are close to the noise level which is precisely what would happen with the pulses obtained in real conditions in field. Then, the PR algorithm with PSO was applied to the remaining signals, 436, first considering that there were two possible types of signals so the k-means algorithm was set to find two clusters. After running the optimization algorithm, one of clusters in the PR map was split into another two well differentiated clusters so the rest of the studies were done with three clusters. The parameters used in the combined PR-PSO algorithm are presented in Table I and the resulting frequency intervals are shown in Table II. The average frequency spectra for the three different types of signals found in the acquisition are plotted in Figure 3. The result was the following PR map in which the three clusters can be clearly defined, Figure 4. The black cluster has 382 elements, the grey cluster 32 and the light grey cluster 22 pulses. The signals corresponding to the black, grey and light grey clusters are shown in Figure 5 from top to bottom, respectively. Plots in Figures 5a and 5b show clear series of pulses with the same delays whereas the

f_T	Clusters	c_1	c_2	Iterations	Swarm size
60 MHz	3	2.05	2.05	200	35

TABLE I: Parameters used in the analysis with power ratios and particle swarm optimization.

f_{1L}	f_{2L}	f_{1H}	f_{2H}
2.4	57.6	58.4	59.2

TABLE II: Frequency intervals in MHz obtained with the combined PR-PSO algorithm to separate the data in three clusters.

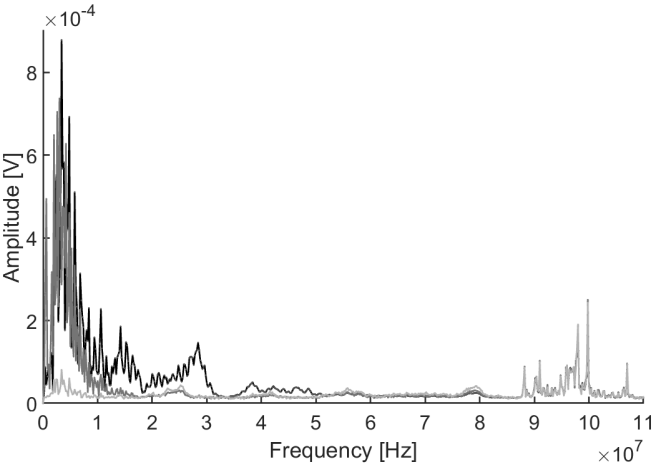

Fig. 3: Averaged frequency spectra for three different types of signals.

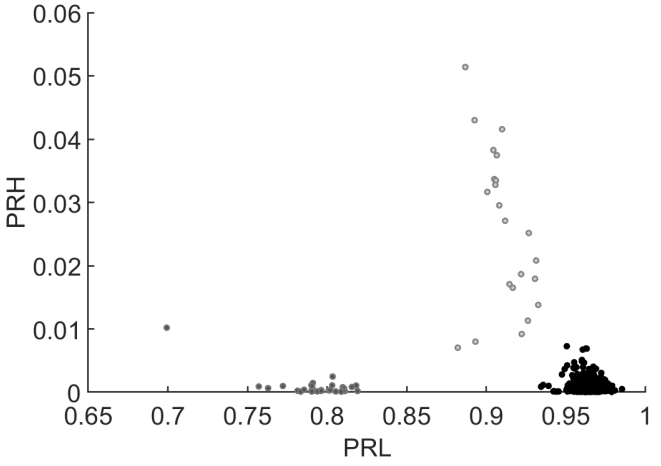

Fig. 4: Power ratio map for signals acquired with the high frequency current transformer.

plot in Figure 5c represents a sample of the signals from the light grey cluster and only has a single pulse. Thus, the first two plots represent PD pulses propagating along the cable and the signal in third plot has to be analyzed further to find its origin. Precisely, the spectra of these latter signals shows that the energy is located mainly in the band from 88 MHz to 108 MHz which corresponds to FM radio signals that are captured by the open shielding of the cable and the HFCT.

C. Localization of multiple sources

Once the signals acquired by the HFCT have been separated it is necessary to apply the TDR technique to the two sets of pulses of interest to determine the positions of the sources. When a PD event takes place in any part of cable, an electromagnetic current pulse is guided through the conductor and propagates away from the point of origin towards both ends of the cable. The location of the PD fault can be determined by considering the relative propagation between the incident and reflected pulses. Assuming a cable of length l, the PD pulse generated from a point P in the middle starts to travel in one direction towards end A to be captured by the sensor at time t_1 after travelling a distance x. At the same time, the PD pulse starts travelling from point P in the opposite direction towards end B of the cable by covering first the distance $l - x$, and then it is reflected back to reach the sensor at end A after a time t_2. The distance of the fault from end A can be calculated with Equation (7):

$$x = l - v\frac{t_2 - t_1}{2} \tag{7}$$

Figure 6 represents a random partial discharge belonging to one of the clusters represented in Figure 4 disregarding the noise. The plot in Figure 6a corresponds to a signal from the black cluster and the plot in Figure 6b to a signal from the grey set. In both cases it is possible to find a first arriving signal labeled with the number 1 and several other pulses that are expected to be reflections. Focusing the study in the top plot, the time difference $t_{21} - t_{11}$ from signals 1 and 2 was found to be 848 ns and substituting this term in Equation (7)

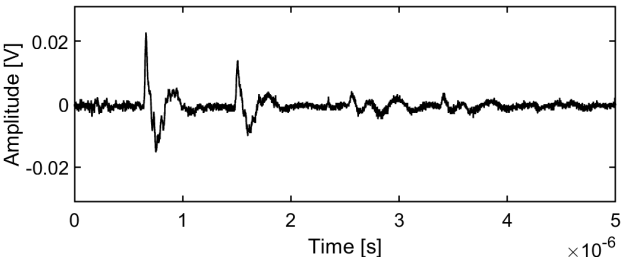

(a) Signal sample of a partial discharge from source 1 yet to be identified.

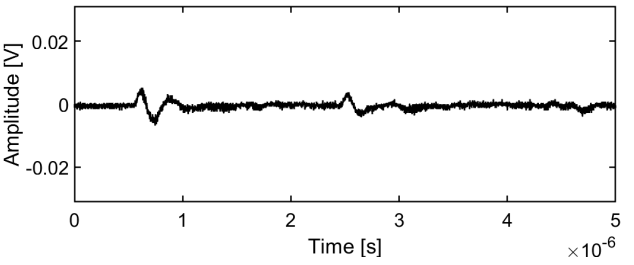

(b) Signal sample of a partial discharge from source 2 yet to be identified.

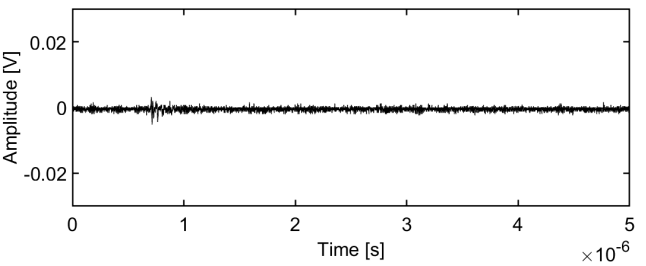

(c) Signal sample identified as noise.

Fig. 5: Samples of the three types of signals.

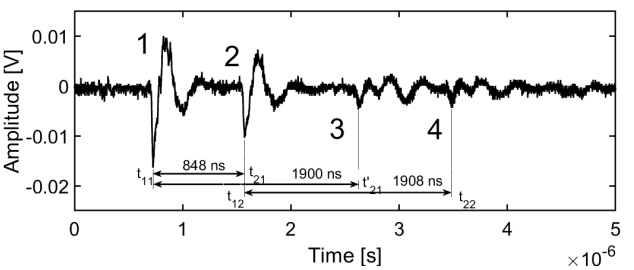

(a) Signal sample of the black set in the PR map and time differences of arrival.

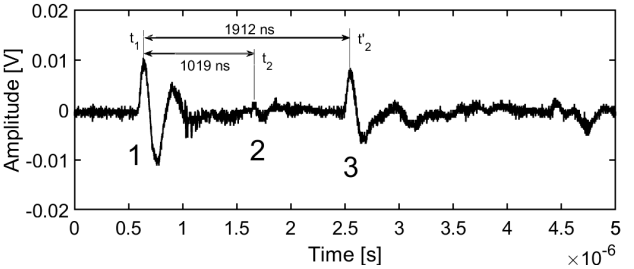

(b) Signal sample of the grey set in the PR map and time differences of arrival.

Fig. 6: Time differences between signals to determine the position of the emission of the partial discharge.

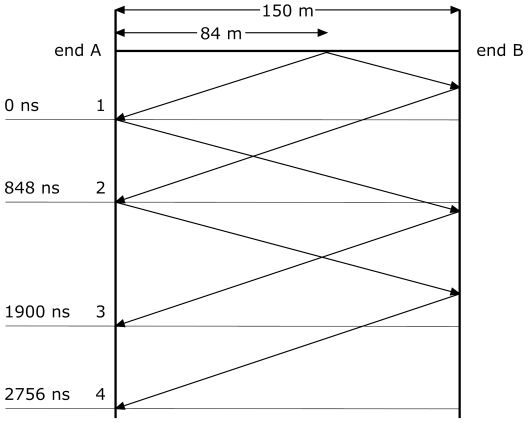

Fig. 7: Lattice diagram for the reflections of the signals in Figure 6a. The horizontal axis is the length of the cable and the vertical axis is time. The origin of time is the arrival of the first signal. The slope of the lines is the inverse of the speed of propagation.

would correspond to a distance of $x_1 = 83.2$ m from end A. Therefore, signal 1 follows a direct path from the induced fault towards the HFCT and signal 2 follows the opposite path from the fault towards end B and is reflected back towards end A, see the lattice diagram in Figure 7. Since end B is open, the reflection coefficient Γ is approximately 1 in Equation (8) where $Z_L \to \infty$ is the load impedance and Z_0 is the characteristic impedance of the cable or transmission line.

$$\Gamma = \frac{Z_L - Z_0}{Z_L + Z_0} \tag{8}$$

The time difference is precisely the time spent in travelling the length of section 2 forward and back. Notice that the signal 2 in this plot is slightly attenuated compared with the signal 1 due to the fact that it has to travel a longer path through a lossy transmission line and it has to be transmitted through the induced fault. This places all partial discharges in the black cluster in the fault located at approximately 84 m from the end A. Additionally, the time difference between signals 1 and 3 is 1900 ns which corresponds to a distance of $299.3 \simeq 300$ m or twice the total length of the cable. Therefore, the signal 1 is bounced back from end A towards end B with a reflection coefficient lower than $|-1|$ because the end A is connected to a voltage source so Z_L would not be infinity. Then, it is transmitted almost completely through the fault at 84 m because the characteristic impedance of the two sections of the cable are the same and it only changes in the portion of cable with the defect. After that, it reaches end B and it is reflected back again towards end A travelling a total of 300 m. The attenuation in this case is much more profound and signal 3 would almost be lost when the amplitude of the discharge is low. Something analogous happens between signals 2 and 4 whose time difference is also equivalent to 300 m, though in this case the number of total reflections in the ends of the cable is increased to three.

Regarding the plot in Figure 6b with pulses from the grey cluster, the time difference between signals 1 and 3 is 1912 ns or $301.1 \simeq 300$ m which is again twice the length of the cable. Therefore, according to Equation (7), the signal 1 is created at end A, acquired directly by the HFCT and transmitted along the cable towards end B, see Figure 8. Additionally, the time difference between signals 1 and 2 is 1019 ns which corresponds to a distance of 160.5 m at the speed of propagation v_m. This is the double distance from end A to the defect in the middle with a 4.7% error, so the signal 2 must be a reflection of the signal 1 in this point due to the slight change in the characteristic impedance of the cable. The reflected signal is very low because the reflection coefficient is low as mentioned before. In summary, the signal 1 departures from end A and before reaching end B, a small part of the signal is reflected back at the defect and the rest is transmitted towards end B. At this point, it is reflected back towards end A travelling a total of 300 m.

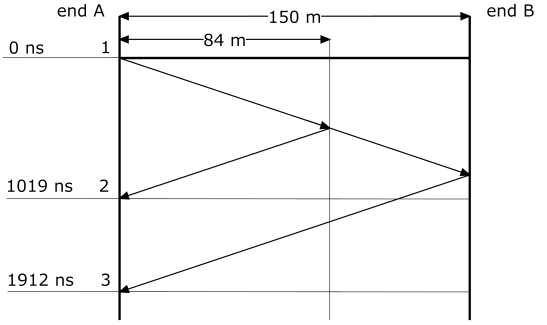

Fig. 8: Lattice diagram for the reflections of the signals in Figure 6b. The slight change in impedance at the fault reflects part of the incident pulse created in end A.

VI. Conclusions

This paper has presented a combined algorithm to extract the frequency characteristics of the pulses in a MV cable and separate them in different classes. The characterization in frequency has been done with power ratio maps and the separation in clusters with particle swarm optimization. An intrinsic characteristic of the method to separate the pulses based on their spectral power is the loss of sensitivity to the polarity of the pulses. Therefore, the method classifies pulses from the same source in the same class even when they have different polarity. Once the pulses have been classified, they are analyzed in the time domain to find the time differences of arrival from the fault to the high frequency transformer connected to one of the ends of the cable.

The performance of the algorithms has been tested with experimental measurements in a cable with a single sensor. The power ratio separation technique detected three types of pulses (in this particular case one of them was noise), so the method has the capability to localize more than two simultaneous PD sources through signal separation prior to the localization with TDR. The position of the defects can be found with high accuracy having an error below 5 % in the worst measured case. The proposed technique can be helpful for PD source localization in different types of insulated power cables, even in facilities with direct voltages, where

the identification of the sources with PRPD patterns is not possible.

Currently, the analysis of the position of the sources of partial discharges is not automatized and the time differences between the first pulse and the reflections are found manually. This visual inspection has been conducted in the plot finding the peaks of the signals but the method can be improved in the future with the use of algorithms to find the onset of a pulse. The Hinkley criterion based on the cumulative energy of the time signal, the Akaike information criterion or the cumulative kurtosis have already been explored by the authors in other papers to detect the onset of the signals [27]. These algorithms are focused on finding the instant when the pulse starts to rise instead of finding the peak of the pulse. Notice that the peak can lead to errors in the measurement of the time differences of arrival due to the dispersion of the pulse in the time domain when the signals are reflected. The effect of the dispersion is a delay in the peak for the reflected signals. Moreover, if the length of the cable is sufficiently short, there may be overlapping of the incident and reflected pulses and it would be necessary to separate them to localize the source. Considering pulses with widths of 500 nanoseconds and a speed of propagation of 1.575×10^8 m/s such as those obtained in this paper, the total length of the cable should be more than 78.75 meters which is usual in real applications of condition monitoring and testing of power cables. There might be another case of overlapping when two or more partial discharges or their reflections happen simultaneously or within the interval determined by the width of the pulse, say those 500 ns. This would only occur when the number of discharges per second is quite high. However, even in those rare cases when the activity is very high, the probability of having two PD from different defects simultaneously in an interval of 500 ns is very low. In any case, the position of the centroid of the cluster in the PR map would be determined by the numerous partial discharges events and the overlapped pulses would be positioned far from the centroids and can be readily discarded. These issues are of interest for further development of the work done in this paper and will be addressed in the future.

ACKNOWLEDGEMENTS

The work done in this paper has been funded by the Spanish Government (MINECO) and the European Regional Development Fund (ERDF) under contract DPI2015-66478-C2-1-R (MINECO/FEDER, UE) and the Academy of Finland under the Grant No. 309412.

REFERENCES

[1] D. Van Hertem and M. Ghandhari, "Multi-terminal VSC HVDC for the european supergrid: Obstacles," *Renewable and sustainable energy reviews*, vol. 14, no. 9, pp. 3156–3163, 2010.

[2] T. K. Vrana and S. Energi, "Review of HVDC component ratings: XLPE cables and vsc converters," in *Energy Conference (ENERGYCON), 2016 IEEE International*. IEEE, 2016, pp. 1–6.

[3] P. S. Georgilakis and N. D. Hatziargyriou, "A review of power distribution planning in the modern power systems era: Models, methods and future research," *Electric Power Systems Research*, vol. 121, pp. 89–100, 2015.

[4] IEC-60885-3:2015, "Electrical test methods for electric cables - part 3: Test methods for partial discharge measurements on lengths of extruded power cables," International Electrotechnical Comission, Geneva, CH, Standard, 2015.

[5] IEC-60071-1:2006, "Insulation co-ordination - part 1: Definitions, principles and rules," International Electrotechnical Comission, Geneva, CH, Standard, 2010.

[6] G. C. Montanari, D. Fabiani, P. Morshuis, and L. Dissado, "Why residual life estimation and maintenance strategies for electrical insulation systems have to rely upon condition monitoring," *IEEE Transactions on Dielectrics and Electrical Insulation*, vol. 23, no. 3, pp. 1375–1385, 2016.

[7] R. Bartnikas, "Partial discharges. their mechanism, detection and measurement," *IEEE Transactions on Dielectrics and Electrical Insulation*, vol. 9, no. 5, pp. 763–808, 2002.

[8] B. Sheng, C. Zhou, D. M. Hepburn, X. Dong, W. Zhou, and J. Yu, "Investigation of partial discharge propagation in cross-bonded HV cable systems," in *2014 IEEE Electrical Insulation Conference (EIC)*, June 2014, pp. 19–23.

[9] T. Hong and M. Fang, "Detection and classification of partial discharge using a feature decomposition-based modular neural network," *IEEE Transactions on Instrumentation and Measurement*, vol. 50, no. 5, pp. 1349–1354, 2001.

[10] H. Nugamani *et al.*, "Investigations on the failure modes of XLPE cables and joints," *IEEE transactions on power delivery*, vol. 13, no. 3, pp. 706–711, 1998.

[11] H. T. Putter, P. Legler, and A. Walker, "Best practices for offline diagnosis of MV cables," in *2017 INSUCON - 13th International Electrical Insulation Conference (INSUCON)*, May 2017, pp. 1–5.

[12] D. Fynes-Clinton and C. Nyamupangedengu, "Partial discharge characterization of cross-linked polyethylene medium voltage power cable termination defects at very low frequency (0.1 Hz) and power frequency test voltages," *IEEE Electrical Insulation Magazine*, vol. 32, no. 4, pp. 15–23, 2016.

[13] A. Saravanakumar, H. Yvonne, K. Gerhard, U. Dirk, and P. Mathias, "Understanding partial discharges in low-power relay and silicone cable modified to suit high-voltage requirement of deep sea electrical system," *International Transactions on Electrical Energy Systems*, vol. 28, no. 6, p. e2542, 2018, e2542 ITEES-17-0497.R1. [Online]. Available: https://onlinelibrary.wiley.com/doi/abs/10.1002/etep.2542

[14] W. M. F. Al-Masri, M. F. Abdel-Hafez, and A. H. El-Hag, "Toward high-accuracy estimation of partial discharge location," *IEEE Transactions on Instrumentation and Measurement*, vol. 65, no. 9, pp. 2145–2153, September 2016.

[15] P. C. Baker, B. Stephen, and M. D. Judd, "Compositional modeling of partial discharge pulse spectral characteristics," *IEEE Transactions on Instrumentation and Measurement*, vol. 62, no. 7, pp. 1909–1916, July 2013.

[16] C. Zhou, M. Michel, D. Hepburn, and X. Song, "On-line partial discharge monitoring in medium voltage underground cables," *IET science, measurement & technology*, vol. 3, no. 5, pp. 354–363, 2009.

[17] M. Wu, H. Cao, J. Cao, H.-L. Nguyen, J. B. Gomes, and S. P. Krishnaswamy, "An overview of state-of-the-art partial discharge analysis techniques for condition monitoring," *IEEE electrical insulation magazine*, vol. 31, no. 6, pp. 22–35, 2015.

[18] H. Ma, J. C. Chan, T. K. Saha, and C. Ekanayake, "Pattern recognition techniques and their applications for automatic classification of artificial partial discharge sources," *IEEE Transactions on Dielectrics and Electrical Insulation*, vol. 20, no. 2, pp. 468–478, 2013.

[19] A. R. Mor, P. H. F. Morshuis, P. Llovera, V. Fuster, and A. Quijano, "Localization techniques of partial discharges at cable ends in off-line single-sided partial discharge cable measurements," *IEEE Transactions on Dielectrics and Electrical Insulation*, vol. 23, no. 1, pp. 428–434, February 2016.

[20] J. Granado, C. Álvarez-Arroyo, A. Torralba, J. Rosendo-Macías, J. Chávez, and M. Burgos-Payán, "Time domain analysis of partial discharges envelope in medium voltage XLPE cables," *Electric Power Systems Research*, vol. 125, pp. 220–227, 2015.

[21] M. Wild, S. Tenbohlen, E. Gulski, and R. Jongen, "Basic aspects of partial discharge on-site testing of long length transmission power cables," *IEEE Transactions on Dielectrics and Electrical Insulation*, vol. 24, no. 2, pp. 1077–1087, April 2017.

[22] V. L. Vigni, A. D. Stefano, R. Candela, and E. R. Sanseverino, "A two-end traveling wave fault location system for MV cables based on LoRa technology," in *2017 IEEE International Conference on Environment and Electrical Engineering and 2017 IEEE Industrial and Commercial Power Systems Europe (EEEIC / I CPS Europe)*, June 2017, pp. 1–6.

[23] G. Y. Kwon, C. K. Lee, G. S. Lee, Y. H. Lee, S. J. Chang, C. K. Jung, J. W. Kang, and Y. J. Shin, "Offline fault localization technique on HVDC submarine cable via time-frequency domain reflectometry," *IEEE Transactions on Power Delivery*, vol. 32, no. 3, pp. 1626–1635, June 2017.

[24] J. Singsathien, T. Suwanasri, C. Suwanasri, S. Ruankon, P. Fuangpian, W. Namvong, P. Saengsaikaew, and W. Khotsang, "Partial discharge detection and localization of defected power cable using HFCT and UHF sensors," in *2017 14th International Conference on Electrical Engineering/Electronics, Computer, Telecommunications and Information Technology (ECTI-CON)*, June 2017, pp. 505–508.

[25] S. Zhe, G. Mengjuan, and W. Qi, "A partial discharge detection and localization system for high voltage cable based on long-tailed sagnac interferometric fiber optic sensor," *Microwave and Optical Technology Letters*, 2017.

[26] J. Ardila-Rey, J. Martínez-Tarifa, G. Robles, and M. Rojas-Moreno, "Partial discharge and noise separation by means of spectral-power clustering techniques," *IEEE Transactions on Dielectrics and Electrical Insulation*, vol. 20, no. 4, pp. 1436–1443, 2013.

[27] G. Robles, J. M. Fresno, and J. M. Martínez-Tarifa, "Separation of radio-frequency sources and localization of partial discharges in noisy environments," *Sensors*, vol. 15, no. 5, pp. 9882–9898, 2015.

[28] G. Robles, J. M. Fresno, J. M. Martínez-Tarifa, J. A. Ardila-Rey, and E. Parrado-Hernández, "Partial discharge spectral characterization in HF, VHF and UHF bands using particle swarm optimization," *Sensors*, vol. 18, no. 3, p. 746, 2018.